Computers in Biology and Medicine 166 (2023) 107455

Contents lists available at ScienceDirect

Computers in Biology and Medicine

journal homepage: www.elsevier.com/locate/compbiomed

Cooperativity and oscillations: Regulatory mechanisms of K-Ras nanoclusters

Manuel Jurado [a], Antonio Zorzano [b,c,d,*], Oscar Castaño [e,f]

[a] Faculty of Pharmacy, University of Barcelona, Barcelona, Spain
[b] Institute for Research in Biomedicine (IRB), Barcelona Institute of Science and Technology (BIST), Barcelona, Spain
[c] CIBER of Diabetes and Associated Metabolic Diseases, Barcelona, Spain
[d] Department of Biochemistry and Molecular Biomedicine, Faculty of Biology, University of Barcelona, Barcelona, Spain
[e] Electronics and Biomedical Engineering, Universitat de Barcelona (UB), Barcelona, Spain
[f] Nanobioengineering and Biomaterials, Institute of Nanoscience and Nanotechnology of the University of Barcelona, Barcelona, Spain

ARTICLE INFO

Keywords:
Cell signaling
Cancer
Ras nanocluster
MAPK pathway
Cooperativity
Computational model

ABSTRACT

K-Ras nanoclusters (NCs) concentrate all required molecules belonging to the extracellular signal-regulated kinase (ERK) mitogen-activated protein kinase (MAPK) pathway in a small area where signaling events take place, increasing efficiency and specificity of signaling. Such nanostructures are characterized by controlled sizes and lifetimes distributions, but there is a poor understanding of the mechanisms involved in their dynamics of growth/decay. Here, a minimum computational model is presented to analyze the behavior of K-Ras NCs as cooperative dynamic structures that self-regulate their growth and decay according to their size. Indeed, the proposed model reveals that the growth and the local production of a K-Ras nanocluster depend positively on its actual size, whilst its lifetime is inversely proportional to the root of its size. The cooperative binding between the structural constituents of the NC (K-Ras proteins) induces oscillations in the size distributions of K-Ras NCs allowing them to range within controlled values, regulating the growth/decay dynamics of these NCs. Thereby, the size of a K-Ras NC is proposed as a key factor to regulate cell signaling, opening a range of possibilities to develop strategies for use in chronic diseases and cancer.

1. Introduction

Cells, through signaling pathways, are able to sense, integrate, and process extracellular information through the plasma membrane, generating robust high-fidelity responses [1,2]. Many of the actors involved in processing and transmitting signals in living cells (signaling proteins, transmembrane receptors, scaffolding proteins, related enzymes, and regulators) are arranged into clusters within, or attached to, cell membranes or the cytoskeleton [3,4]. Some examples are G-protein clusters, integrin clusters, ion channel clusters, and heparan sulfate glycomimetic clusters, among others. These clusters present a versatile structure, which can consist of homo- or hetero-oligomers, or they can be arranged by scaffolding proteins that join proteins together [4–6]. Furthermore, the clusters are dynamic structures that vary over time and space and are organized on length scales from nanometers to micrometers [7,8]. In detail, nanoclusters (called from now on as NCs) concentrate signaling events in a delimitated small area, increasing the efficiency and specificity of the signaling pathway [2,9–12]. Each type of nanocluster receives different inputs and provides specific outputs [4,13].

Ras NCs are a type of G-protein clusters that constitute finite and transient signaling nanoplatforms that are made up of linked Ras proteins, distributed along the plasma membrane [2,11], which trigger the cell signal transduction process [14–16]. These NCs are found in the extracellular signal-regulated kinase (ERK) mitogen-activated protein kinase (MAPK) signaling pathways, where the signal transduction process starts when growth factors activate receptor tyrosine kinases (RTKs) on the cell membrane and the further G-proteins Ras, triggering a cascade of activations of three kinases: Raf, MEK-1/2 and ERK-1/2 [14,15,17–39]. These three kinases drive extracellular signals across the plasma membrane and to the inner of the cell. Upon stimulation with the epidermal growth factor (EGF), the double phosphorylated ERK-1/2 ($_{pp}$ERK-1/2) is delivered to the cytosol and reaches the nucleus of the cell, collaborating in the regulation of the cell activity [24–27,40,41].

* Corresponding author. Institute for Research in Biomedicine (IRB), Barcelona Institute of Science and Technology (BIST), Barcelona, Spain.
E-mail address: antonio.zorzano@irbbarcelona.org (A. Zorzano).

https://doi.org/10.1016/j.compbiomed.2023.107455
Received 28 November 2022; Received in revised form 7 August 2023; Accepted 4 September 2023
Available online 9 September 2023

Each type of Ras isoform (H-, N- and K-Ras) is associated with a different type of Ras NC, with specific characteristics, such as controlled lifetimes and sizes. In the case of K-Ras NCs, which are the focus of the present study, they present lifetimes experimentally measured between 0.1 s and 1.0 s (describing a distribution with its maximum at 0.5 s), and sizes ranged between 5 and 10 Ras molecules (although the most predominant values are 6–7 K-Ras proteins) [4,6,11–13,42].

K-Ras NCs present a rather ultrasensitive stimulus/response behavior, which is used by cells to convert analog extracellular stimuli into digital intracellular responses [2,11,12]. Such behavior is the result of combining signaling events spatially distributed within NCs and birth/death dynamics dependent on the local NC production ($_{pp}$ERK-1/2). Thus, a robust and high-fidelity response is provided without invoking sophisticated cascade structures or a mesh of regulatory feedback/feedforward loops between the elements of the pathway [2].

The time response of a K-Ras NC (mainly its duration and amplitude) influences cell fate and production [2]. And considering that uncontrolled signaling transduction leads to cell disorders and diseases, such as the proliferation of tumors [43–46], modulating the time pattern of K-Ras NCs (i.e., the distributions of sizes and lifetimes of activated K-Ras NCs) can help in developing strategies to fight against cellular disorders. Some advances made recently help to understand the formation and the spatial organization of these nanostructures, and some mechanisms involved in their activity. Unfortunately, there is an unknown in the mechanisms that drive their structural regulation, and their size and lifetime distributions [6,47].

Ras NCs are considered structures where activation and conformational changes of the stimulated molecules promote cooperativity, increasing the sensitivity of neighboring molecules and resulting in efficient signal transduction [3,15,48,49]. The formation and growth of clusters are modulated by cooperative binding, meaning that molecular affinity within a cluster increases with cluster size [4,49]. Indeed, with sufficient binding cooperativity, binary signaling (understood as the possibility of switching rapidly between a low "off" and a high "on" states or levels) is triggered in Ras NCs and, thereby, the signal fidelity increases as a function of the cluster size [12]. Improvements in molecular dynamics studies show that bidirectional cooperativity (cooperative binding and dissociation) regulates the dynamics of these nanodomains, where the number of available neighboring molecules modulates both binding and dissociation probabilities.

A model approach to the growth/decay dynamics of the EGF\K-Ras \ERK-1/2 MAPK signaling pathway was proposed to shed light on the regulation of the size and lifetime distributions of K-Ras NCs. The most novel aspect that the model provides is to define the NCs as dynamic and cooperative structures with the speeds of their growth and decay reactions dependent on their sizes, without fixing any kinetic value. Here we provide computational evidence that K-Ras NCs promote their own growth and local production positively dependent on their current sizes, whilst their lifetime is inversely proportional to their sizes. Furthermore, the cooperativity induces oscillations in their size distributions, keeping sizes and lifetimes bounded between controlled values, for a wide range of kinetic parameters. Therefore, the obtained results suggest K-Ras NCs as signaling nanostructures that self-regulate their growth/decay dynamics through controlled sizes, proposing this regulation as a strategy to modulate the MAPK response and the cell fate decision.

2. Methods

2.1. Model

The proposed model of reference corresponds to a simplified version of the three-step EGF\K-Ras\ERK-1/2 MAPK cascade [14,15], considering the different signaling processes, from their activation upon EGF stimulation to the production of the $_{pp}$ERK-1/2 output response, carrying out the recruitment and the activation/deactivation processes of the intermediate signaling messengers (Raf-1 and MEK-1/2), but organized in K-Ras NCs (Fig. 1A). Basically, the model consists of spatially distributed and dynamic signaling nanoplatforms of clustered K-Ras proteins along the plasma membrane, where signaling events are triggered independently within each NC (Fig. 1B). The EGF stimulus activates the fraction of K-Ras monomers capable of forming NCs or clustering with existing ones [49,50]. And signaling substrates are integrated into structures forming a complex of Raf-1\MEK-1/2\ERK-1/2, which are recruited into each K-Ras NC and activated during its lifetime (Fig. 1A). Each K-Ras NC provides a self-regulating process of its lifetime, dependent on its local output production ($_{pp}$ERK-1/2) and triggered by a negative feedback loop from its output to the K-Ras clustering level [2] (Fig. 1). The local $_{pp}$ERK-1/2 expression of each active K-Ras NC is proportional to its size [2], and the overall sum of all these local $_{pp}$ERK-1/2 productions constitutes the output cell response [11] (Fig. 1).

The experimental values of the expressions of the components that build up the model correspond to those described in the literature [15,26], which are still accepted in recent research [4,6]. In a real scenario, concentrations of 3.87×10^6 K-Ras monomers, 3.7×10^5 molecules of Raf, 2.2×10^7 molecules of MEK, and 2.1×10^7 molecules of ERK distributed in the cytosol have been observed (Suppl. Table I). [15,26,50]. These values are relatively high when compared to the concentration of active K-Ras molecules accessible on the plasma membrane of BHK cells capable of clustering, which is around 8×10^5 molecules [49,50]. This concentration has been used as an input parameter for the proposed model. Notice that all substrate elements (Raf, MEK, ERK) are present in enough concentrations compared to the available K-Ras proteins so as to not limit any reaction of the proposed model. In addition, a maximum external stimulus EGF has been considered in order to analyze the model under maximum signal conditions and, thereby, considering a maximum number of active NCs.

The proposed model of K-Ras NCs consists of 5 reactions (Suppl. Table III): two of them (those related to the NC formation and the NC dissociation) were expressed independent of the K-Ras NC's size (the amount of clustered K-Ras molecules); and the other three (those concerning the internal K-Ras binding, dissociation and $_{pp}$ERK-1/2 production processes) were defined dependent on the current size of the K-Ras NC (Suppl. Table II).

On one hand, regarding the independent reactions, the NC formation (a_1) was defined according to the expression of active K-Ras monomers available in a cell, whilst the NC dissociation (a_5) was regulated directly by the local output response ($_{pp}$ERK-1/2), and thereby, indirectly by the size of the K-Ras NC [2] (Suppl. Table III). Their corresponding constant rates (k_1 and k_5) were defined with a wide range of values to measure their influence on the tuning level of the sizes and lifetimes distributions of K-Ras NCs, as well as to analyze the robustness of the proposed model against kinetic variations (Suppl. Table II). Notice that realistic values of these constant rates following reported values in previously published research [2,35,49,50] have been included, which were defined from real measures or, failing that, suggested as biochemical estimations. Thus, the constant rate that triggers the K-Ras dimerization (k_1), and therefore the formation of the basic structure of a NC, was reported to be around 0.5 s^{-1} [4,51–54], and in the present study, this parameter has been defined in the range of 0.1–1.0 s^{-1}. Similarly, the constant rate that regulates the NC dissociation (k_5) was tuned in 2.0 s^{-1} [2,50] to adjust the estimated average lifetime of 0.5 s for K-Ras NCs, whereas it has been defined in the range of 0.01–10.0 s^{-1} to develop the present study.

On the other hand, the reactions dependent on the K-Ras NC size express a high level of self-regulation. In addition, they are defined through the Heaviside step function, which suggests a high cooperative behavior within each K-Ras NC (eq. 1- eq. (3)) [55,56].

These reactions constitute the NC growth (a_2) that consists of the aggregation of a new active K-Ras molecule into the existing NC and therefore, an increase of its size; the NC decay (a_3) that represents the loss of a clustered K-Ras molecule and thereby, a decrease of the NC size; and the production of local $_{pp}$ERK-1/2 (a_4), which is proportional to the

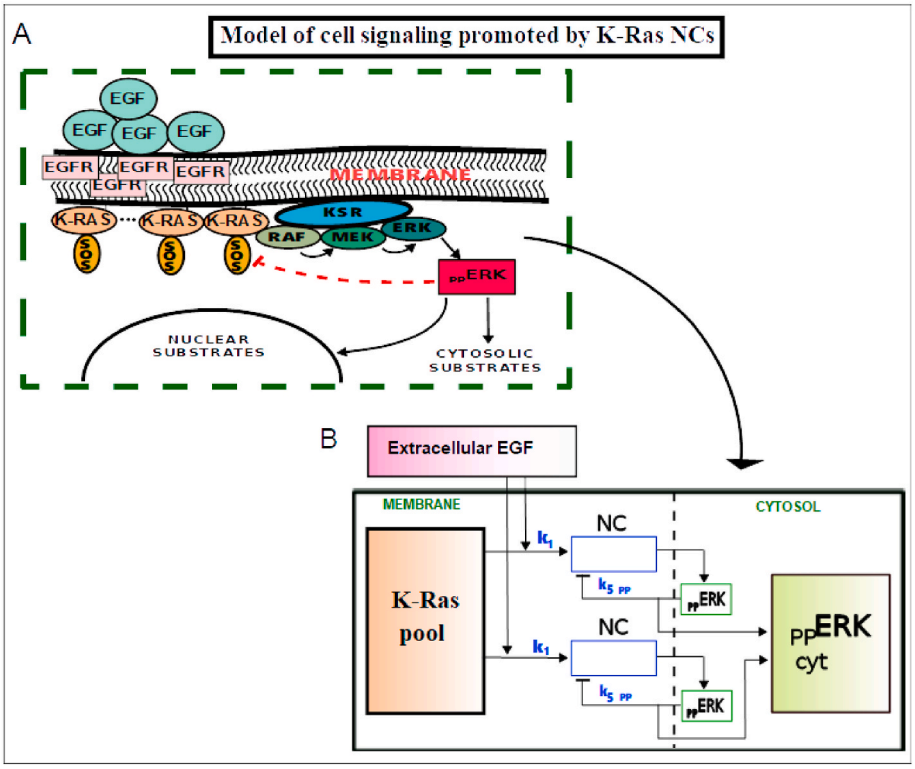

Fig. 1. Schematics of K-Ras NCs model for cell signaling. A) Representation of a K-Ras NC module formed by different molecules of K-Ras (an average of 5–10 K-Ras) that become anchored and clustered to the cell membrane after being activated by extracellular EGF, which is picked up by its receptor (EGFR). Son of sevenless (SOS) is a guanine nucleotide exchange factor that facilitates such activation and promotes cooperativity for K-Ras clustering in the plasma membrane. After the formation of a K-Ras NC, a substrate structure promoted by the scaffolding protein Kinase Suppressor of Ras (KSR) is recruited from the cytosol, integrating the different substrates (Raf-MEK-ERK) required by the K-Ras NC to transduce the extracellular signal into the cell, during its lifetime. Upon activation, the NC generates a local concentration of double phosphorylated ERK ($_{pp}$ERK), which is finally delivered to the cytosol and the cell nucleus, which triggers the activation of specific substrates. B) Schematic model of a cell signaling system based on K-Ras NCs activated by the extracellular stimulus EGF. K-Ras molecules are activated by nearby EGF located in the cell membrane, becoming clustered and forming distributed NCs along the plasma membrane. Each of these NCs generates a local production of double phosphorylated ERK molecules ($_{pp}$ERK), and the overall sum of all these local productions in the plasma membrane constitutes the output cell response (cytosolic $_{pp}$ERK) (color version required for printing).

NC size [2] (i.e. the NC generates one $_{pp}$ERK-1/2 per each clustered K-Ras). These three reactions were defined through specific and constant rates in previously published research [2,15,26,49,50], but without establishing a unified criterion. Thus, rates compressed between 0.1 and 10.0 s^{-1} for the forward association and backward dissociation reactions were considered. In addition, catalytic constant rates corresponding to kinase phosphorylation processes were considered larger, between values of 10.0 and 100.0 s^{-1}. A novel concept in the definition of these reactions has been introduced in the present study, expressing them as a function of the current size of the K-Ras NC at any moment throughout its lifetime (eq. 1- eq. (3)). This represents the main contribution of the proposed model, which aims to define a K-Ras NC as a dynamic structure that self-regulates its growth and decay according to its size, allowing a reasonable explanation for the empirical results that report regulated sizes and lifetimes of this kind of NCs [42,49,50] without recurring to fix kinetic parameters and a collection of boundary conditions in the model. Despite this variability in the kinetic parameters, the fixed values used in previous studies are included in the range of values considered in the proposed model.

The description of these reactions presents two novel particularities: i) their rates are variables expressed as a function of the K-Ras NC size and ii) their rates are defined through the Heaviside step function or its inverse version, depending on the reaction.

K-Ras NC growth reaction: $a_2 = k_2 \cdot H\_1(x)$, where $k_2 = size$ (1)

K-Ras NC decay reaction: $a_3 = k_3 \cdot H\_2(x)$, where $k_3 = 4 \cdot size^2$ (2)

K-Ras NC local production reaction: $a_4 = k_4 \cdot H\_3(x)$, where $k_4 = 4 \cdot size$ (3)

where H_1 denotes the inverse of the Heaviside step function, and H_2 *and* H_3 denote the Heaviside step function:

$H\_1(x)$ from eq. 1 $\rightarrow H\_1(x) := 1_{x \leq Nsig}$ (4)

$H\_2(x)$ from eq. 2 $\rightarrow H\_2(x) := 1_{x \geq Nsig}$ (5)

Defining these reactions through the Heaviside step function, or its inverse, suggests a highly cooperative behavior within each K-Ras NC. Indeed, the expression of the reactions related to the growth and decay of a K-Ras NC (eq. (1), eq. (2)) through the Heaviside step function (eq. (4), eq. (5)) allows defining bidirectional cooperativity, switching between cooperative binding (related to the clustering of free active K-Ras into a NC) and dissociation processes (related to clustered K-Ras within the same NC) with a probability of occurrence modulated by the number of clustered K-Ras molecules within the same NC. Thus, the occupancy of neighboring sites into the NC increases when its size is below an optimal size (N_{sig}) (eq. (1), eq. (4)), but when this value is reached, the probability of dissociation takes relevance (eq. (2), eq. (5)).

In addition, the lifetime of each K-Ras NC has been defined as inversely proportional to the root of its size, reflecting higher chances of dying with increasing sizes (lifetimes distribution of K-Ras NCs fits better to τ when the local production reaction of each nanostructure is defined in terms of $\sqrt{(size)^{-1}}$, rather than $size^{-1}$, $size$ or $size^2$; data not shown). This condition has been reflected through the argument of the step function from eq. (3):

$H\_3(x)$ from eq. 3 $\rightarrow H\_3(x) := I_x \geq \binom{-1/2}{size}$ (6)

This equation (eq. (6)) reveals higher choices of local $_{pp}$ERK-1/2 production with the increase of the K-Ras NC size [2]. Therefore, this increase in the $_{pp}$ERK-1/2 expression promotes the activation of the self-regulation mechanism from the disassembly reaction a_5 [2].

A schematic representation of the distinct available states of a K-Ras NC is represented in Fig. 2, depending on the different reactions that can be triggered (NC formation, K-Ras binding into a NC, K-Ras dissociation from a NC, local $_{pp}$ERK-1/2 production, and NC death).

There is published literature focused on the link between protein clustering and the Heaviside function [55–61], mainly to express that proteins are segregated inside clusters. Hence, a relation between cooperativity, Ras clustering, and its mathematical description through the step function may be suggested in our model.

Experimentally, cooperative behavior in K-Ras NCs was reported, increasing in size as more clustered K-Ras molecules are present (cooperative binding) [12]. On the other hand, it was observed that K-Ras NCs increase until reaching a limited size (N_{sig}) within the range of 5–10 Ras molecules (N_{sig} is considered 10 K-Ras molecules for the present study). Furthermore, the lifetime of these nanostructures (τ, defined as the current time comprised between the K-Ras NC generation and its death) presents a normal distribution with an average value of about 0.5 s *in vivo* [35,50]. All these conditions concerning the growth and death of K-Ras NCs were aimed to be represented with the above equations (eqs. (1)–(3)), presenting K-Ras NCs as self-regulated signaling structures, promoting cooperativity between their constituents and limiting their lifetime and growth through their own size. After checking different options to define the rates of the aforementioned reactions (k_2, k_3, and k_4 defined with different fixed values; not all data are shown, but some examples are represented in Suppl. Fig. 9), the best results to fit the size and lifetime distributions of K-Ras NCs close to the expected values were obtained defining these reaction rates as variables, in terms of the current size of each active K-Ras NC (Suppl. Table II).

2.2. Simulations

All the simulations were developed using a stochastic approach similar to Gillespie's Stochastic Simulation Algorithm (SSA), treating the model reactions as a group of stochastic events [62–64]. The different signaling events were defined as Poissonian processes with a frequency characterized by the corresponding reaction rates. And the signaling model of K-Ras NCs was implemented in the Fortran programming language. Each K-Ras NC was simulated in time considering different ranges of the parameters k_1 and k_5, and stimulated by the maximum expression of the input stimulus EGF:

- Input stimulus rate $\alpha = EGF/EGF_{max} = 1$
- $k_1 \in [0.1 - 1.0]\ s^{-1}$
- $k_5 \in [0.01 - 10.0]\ s^{-1}$

k_1 was varied in steps of 0.1 s^{-1} within the range of values from 0.1 to 1.0 s^{-1}. And k_5 was varied in proportional steps depending on the considered range (steps of 0.05 s^{-1} between the range 0.01–0.1 s^{-1}; steps of 0.1 s^{-1} between the range 0.1–1.0 s^{-1}; and steps of 1.0 s^{-1} between the range 1.0–10.0 s^{-1}). However, the rest of the kinetic parameters which depend on the current size of the NC were updated at each simulation moment according to its definition (Suppl. Table II).

Thus, varying the values of the two kinetic constants k_1 and k_5, and defining the rates belonging to the rest of the reactions of the model in terms of the current size of K-Ras NCs (Suppl. Table II and eqs. (1)–(3)), it is possible to evaluate the time evolution of the sizes and lifetimes of K-Ras NCs. Since the kinetic parameters of the model have not been fixed to specific values, the observed robustness of K-Ras NCs can be demonstrated without resorting to fixed kinetic constants or boundary conditions, as has been applied in studies published to date.

The simulations were carried out for enough time to ensure a representative simultaneous population of active K-Ras NCs (greater than 10,000) to be in accordance with a realistic situation [35,50]. And such a condition was achieved with simulations of 10 s. Although it could be possible to simulate the model until expiring all the initial pool of K-Ras monomers, since they are degraded after the dissociation of the nanostructure where they were clustered, it did not alter the final patterns of sizes and lifetimes distributions of the nanostructures (data not shown).

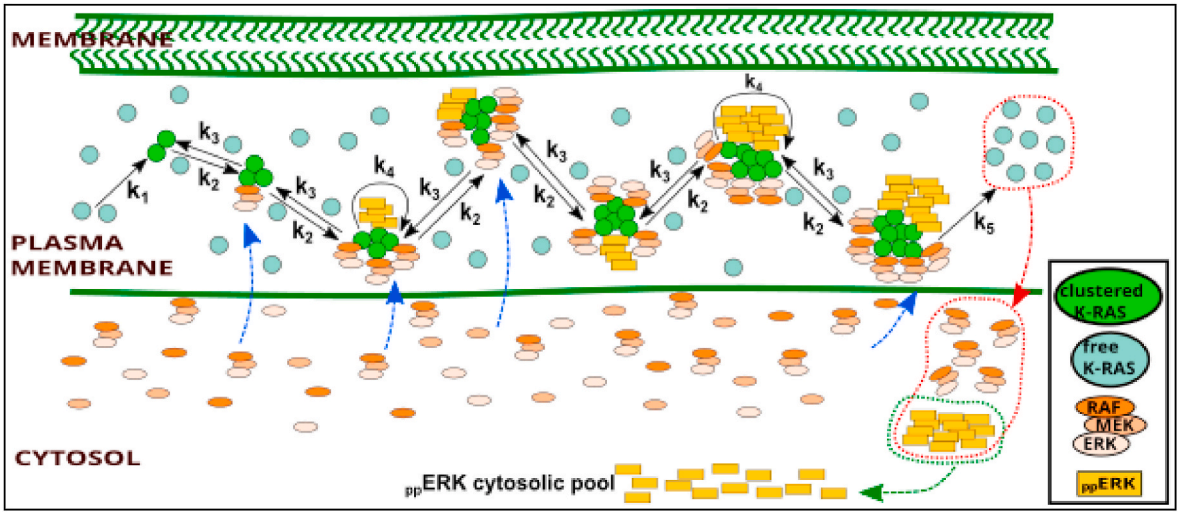

Fig. 2. Schematic representation of the states and reactions of the proposed model. Representation of different states of a K-Ras NC constituted by different numbers of clustered K-Ras proteins. Active free K-Ras proteins are dispersed along the plasma membrane, which can get clustered forming a new NC (reaction driven by kinetics k_1) or clustered in an existing NC (reaction driven by kinetics k_2), increasing its size. Besides, an already clustered K-Ras protein can be released to remain dispersed in the plasma membrane (reaction driven by kinetics k_3), decreasing the size of the K-Ras NC. Meanwhile, substrate complexes made of Raf-MEK-ERK kinases can be recruited from the cytosol to the plasma membrane and activated in a K-Ras NC for further signaling processes (process represented by the dashed blue lines). At this point, the clustered K-Ras proteins promote the phosphorylation of these kinases, leading to the local production of active ERK ($_{pp}$ERK), which represents the output of the EGF/K-Ras/ERP MAPK pathway (this activation process is represented by kinetics k_4). Finally, when enough $_{pp}$ERK production is reached, the NC has the chance of disassembling (reaction driven by kinetics k_5), and then K-Ras, Raf, MEK, ERK, and $_{pp}$ERK are segregated to the cytosol (process represented by the dashed red and green lines) (color version required for printing).

In order to characterize the sizes and lifetimes distributions of K-Ras NCs, depending on the values of k_1 and k_5, both the normalized distribution of K-Ras NCs as a function of their *sizes* and the normalized distribution of K-Ras NCs as a function of their *lifetimes* were carried out. The reported values of sizes and lifetimes refer to their values at the time of NCs' death. In addition, average and maxima values of both K-Ras NCs' sizes and lifetimes were analyzed, as a function of both k_1 and k_5 parameters.

3. Results

The distributions of signaling K-Ras NCs belonging to the EGF\K-Ras \ERK-1/2 MAPK route were measured as a function of their sizes and lifetimes, depending on the values of the constant rates k_1 and k_5, for a maximum input stimulus (Figs. 3–10). In short, defining the internal reaction rates of K-Ras NCs as cooperative processes dependent dynamically on their actual sizes (eqs. (1)–(3)), the lifetimes and sizes of the nanostructures can be limited within well-defined ranges, according to the results observed experimentally and published in the scientific literature [35,50]. Indeed, the average lifetimes of K-Ras NCs are mainly ranged between 0.5 s and 3.0 s, although for the great range of the k_1 and k_5 values the average values of lifetimes are ranged between 0.5 s and 1.5 s (Fig. 3). In addition, the lifetimes with maximum distributions of K-Ras NCs are ranged between 0.6 s and 1.8 s (Fig. 4). On the other hand, the average K-Ras NCs sizes at the death moment are mainly ranged between 3 K-Ras and 5 K-Ras, although for low values of k_1 and k_5 average sizes of 7 K-Ras are reached (Fig. 5A). However, when talking about average K-Ras NCs maximum sizes, their values increase up to 9 K-Ras, also for low values of k_1 and k_5 (Fig. 5B). Furthermore, the sizes with maximum distributions of K-Ras NCs are ranged between 2 K-Ras and 10 K-Ras (Fig. 6).

Analyzing in more detail the obtained results, considering fixed k_1 while varying k_5, the K-Ras NCs lifetimes describe a right-skewed distribution (like a lognormal distribution) that remains controlled and ranged between the values of 0.5 and 3.0 s, considering most of the values of k_5. In fact, the pattern of this distribution does not show relevant changes when modifying k_1, but becomes tighter with higher k_5, ranging most lifetimes between 0.5 and 1.5 s. And, its maximum expression is close to τ, exactly between 0.5 and 1 s (Fig. 7).

On the other hand, when varying k_1 while fixing k_5, the K-Ras NCs lifetimes also describe a right-skewed distribution that remains controlled and ranges between mainly the values of 0.5 and 4.0 s, although the NCs' lifetimes for the majority of k_5 values are concentrated below 2 s. And this distribution spreads out as k_1 increases, presenting more expression of K-Ras NCs with larger lifetimes (Fig. 8).

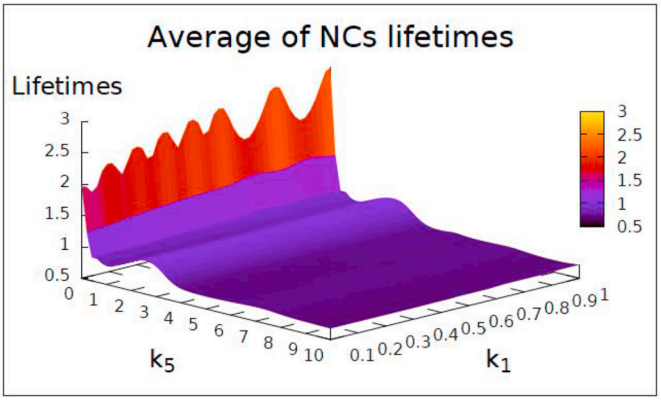

Fig. 3. 3D representation of average NCs lifetimes as a function of k_1 and k_5 values. Average lifetimes of active K-Ras NCs for the full considered ranges of values of k_1 ([0.1–1.0] s^{-1}) and k_5 ([0.01–10.0] s^{-1}). The average lifetimes of K-Ras NCs are ranged from 0.6 to 1.8 s (color version required for printing).

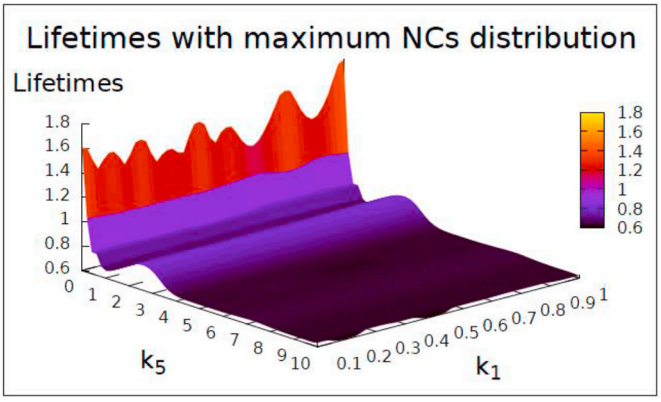

Fig. 4. 3D representation of NCs lifetimes with maximum K-Ras NCs distributions, as a function of k_1 and k_5 values. Lifetimes of active K-Ras NCs that present maximum distributions of NCs, for the full considered ranges of values of k_1 ([0.1–1.0] s^{-1}) and k_5 ([0.01–10.0] s^{-1}). These lifetimes with maximum K-Ras NCs distributions are ranged from 0.5 to 3.0 s (color version required for printing).

Regarding the distribution of the K-Ras NCs sizes, when fixing k_1 while varying k_5, it spreads out but remains well ranged between 2 and 9 K-Ras molecules, regardless of the k_5 increment. What is certain is that the greatest extension of NCs is concentrated between the sizes of 2–5 K-Ras molecules (Fig. 9). Considering the distribution of NCs related to their maximum sizes (which can be different from those of that the time of NC's dissociation), some nanostructures can reach sizes of up to 11 K-Ras proteins, although the distribution becomes narrower and concentrates around 3-8 K-Ras molecules as k_5 increases (Suppl. Fig. 3).

When varying k_1 while fixing k_5, the distribution of K-Ras NCs sizes also describes a right-skewed pattern (like a lognormal one), ranging the great extension of nanostructures between 2 and 8 K-Ras molecules. And the highest expression of K-Ras NC is concentrated in lower sizes as k_1 increases, reducing the range of its dispersion, regardless of the value of k_5 (Fig. 10). Concerning the distribution of NCs related to their maximum sizes, it also describes a right-skewed pattern that reaches values of up to 11 K-Ras proteins, although this distribution is concentrated at lower maxima sizes compressed between 2 and 8 K-Ras molecules as k_1 increases (Suppl. Fig. 4).

Regarding the evolution of $_{pp}$ERK-1/2, it describes a predictive pattern according to the variation of parameters k_1 and k_5. Thus, the expression of $_{pp}$ERK-1/2 is reduced as k_5 increases, since NCs require less local $_{pp}$ERK-1/2 to trigger its self-regulated mechanism responsible for its own decay. In turn, the lifetime of NCs is reduced since these nanostructures reach the proper conditions to disappear in less time (Suppl. Fig. 5). However, as k_1 increases, the production of $_{pp}$ERK-1/2 accelerates and it reaches its higher expression in less time, because the activation of K-Ras monomers and the generation of NCs accelerate, allowing the last ones to reach sufficient sizes in less time, with local ppERK-1/2 production proportional to these sizes (Suppl. Fig. 6). In this case, the lifetime of these nanostructures is reduced as well since enough $_{pp}$ERK-1/2 expression is achieved in shorter times to trigger its decay until disappearance.

Concerning the time evolution of the current active NCs, their number is higher when k_1 increases and when k_5 decreases. Both situations yield, from a probabilistic point of view, an increase in the generation of NCs and a decrease in the dissociation rate of NCs, respectively (Suppl. Figs. 7 and 8). Thus, with low values of k_5, K-Ras NCs require a higher amount of $_{pp}$ERK-1/2 to trigger its decay, and thereby the number of active NCs is accumulated during the simulation time. After a certain time, these NCs have enough $_{pp}$ERK-1/2 and their rate of decay increases, presenting more chances of disappearance and reducing its amount along the simulation time. In addition, with high values of k_1, the generation of new K-Ras dimers accelerates and

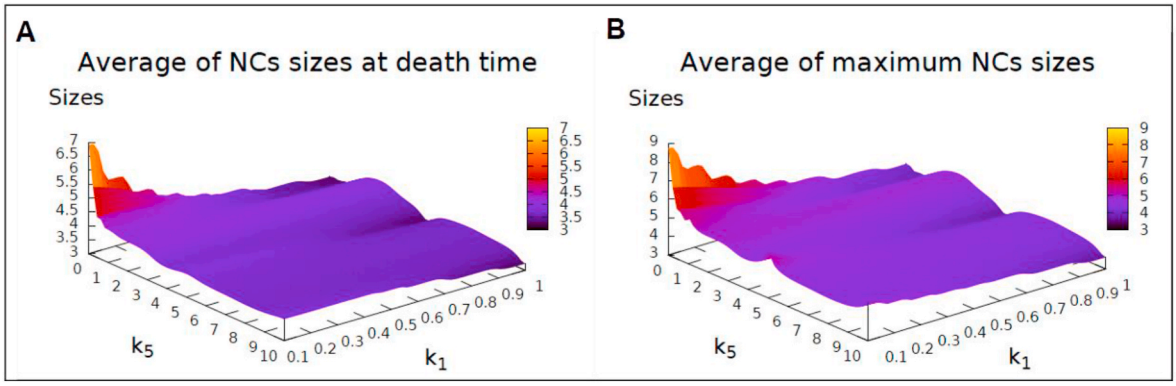

Fig. 5. 3D representation of average NCs sizes as a function of k_1 and k_5 values. A) Average sizes of active K-Ras NCs at disassembly time, for the full considered ranges of values of k_1 ([0.1–1.0] s^{-1}) and k_5 ([0.01–10.0] s^{-1}). The average sizes of K-Ras NCs are ranged from 3 to 7 K-Ras proteins. B) Average of maximum sizes of active K-Ras NCs, for the full considered ranges of values of k_1 ([0.1–1.0] s^{-1}) and k_5 ([0.01–10.0] s^{-1}). The average sizes of K-Ras NCs are ranged from 3 to 9 K-Ras proteins (color version required for printing).

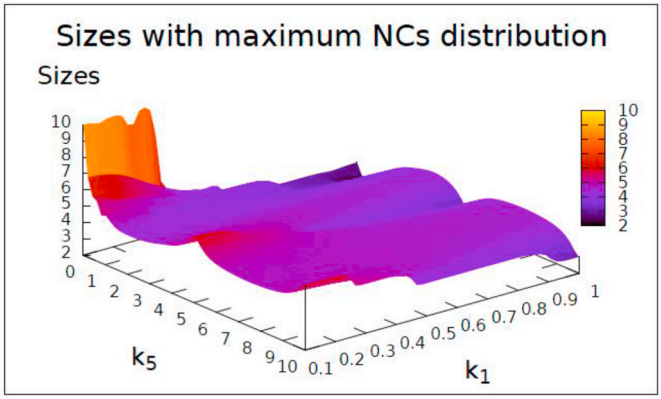

Fig. 6. 3D representation of maximum NCs sizes as a function of k_1 and k_5 values. Lifetimes of active K-Ras NCs that present maxima distributions of NCs, for the full considered ranges of values of k_1 ([0.1–1.0] s^{-1}) and k_5 ([0.01–10.0] s^{-1}). These average sizes with maxima K-Ras NCs distributions are ranged from 2 to 10 K-Ras proteins(color version required for printing).

thereby, many active NCs with a probability of growing is concentrated in shorter times. These NCs are able of generating enough local $_{pp}$ERK-1/2 expression to activate its decay mechanism from short simulation times, and therefore the distribution of the current active NCs is reduced over the simulation time.

4. Discussion

We provide computational evidence for describing K-Ras NCs as cooperative signaling structures that self-regulate their growth and local output, at the same time keep controlled their sizes and lifetimes on specific ranges. Furthermore, one aspect that provides credibility to the model is that the obtained results for K-Ras NC sizes and lifetimes closely match values from experimental observations reported in the literature [35,50].

This behavior of the K-Ras NCs arises from considering two novel and unusual ideas when defining the proposed model: i) each K-Ras NC is considered a cooperative structure that promotes its own growth and its local production, and ii) the K-Ras NC growth/decay and its local production depend on its actual size. The first concept is incorporated into the model by defining the reactions in terms of the Heaviside function to reflect that proteins segregate into clusters. And the second concept represents an unusual way of defining the inner reaction rates belonging to the K-Ras NCs dynamics: each rate depends directly on the size of the K-Ras NC at each moment. This idea allows us to describe the NCs as structures that self-regulate based on their own evolution in terms of their sizes. In fact, this idea represents a groundbreaking and non-conditional way of defining NCs. So far, these structures have been described in general terms with reactions having probabilities of occurrence defined by fixed kinetic values. This practice forces us to limit the computational models to very strict ranges of kinetic values while incorporating many constraints and boundary conditions, in many cases assumed. However, defining the reactions of the NCs referred to their growth and decay through a non-fixed manner allows us to predict the behavior of these clustered structures without imposing ranges of kinetics values, which may be difficult to measure experimentally.

If a stochastic approach to the computational model is included in addition, where the probabilities of occurrence of each reaction are established as the simulation evolves, depending on the kinetic parameters of the model and its boundary conditions, rather than requiring a deterministic point of view where the reactions develop in a pre-established order, the level of self-regulation of the defined cellular system is multiplied.

Unexpectedly, from the simulations was observed that oscillations in the sizes of K-Ras NCs arise along their lifetimes, which control their local output and their chances of collapsing. This oscillating pattern arises when the rate of NC dissociation (k_5) is varied, causing nanostructures to restrict their sizes and avoid uncontrolled dispersion. Thus, if the expected pattern of the sizes distribution is to increase while k_5 decreases, the K-Ras NCs change this growing trend and modulate the number of proteins that make them up, alternating periods of increase and decrease of their sizes, and thereby allowing to remain a distribution of these nanostructures within a controlled range of sizes. This effect is more easily observable at low k_1 values since the spread of size values is likely to increase due to the need for more time to reach enough local production by the K-Ras NC (Suppl. Figs. 1 and 2). But in all, the decay process of NCs is a key factor in the dynamics of these nanostructures, since it depends on the local $_{pp}$ERK-1/2 production, which in turn is proportional to their actual size [2].

Apart from obtaining average values of NCs lifetimes and sizes according to experimental values reported in the literature (Figs. 3 and 5, respectively), simulations reveal that an accurate fitting of the sizes and lifetimes distributions of the K-Ras NCs was achieved, without presenting an uncontrolled scattering of their values, even considering wide ranges of kinetic parameters (Figs. 7–10). The model predicts that the K-Ras NCs sizes fit a lognormal distribution ranging between 2 and 9 K-Ras molecules, but the greatest extension of NCs is concentrated between the sizes of 2 and 5 K-Ras molecules. In addition, the K-Ras NCs lifetimes also describe a lognormal distribution where most lifetimes remain controlled and ranged between the values of 0.5 and 2.0 s, but its maximum expression is concentrated between 0.5 and 1.0 s. These

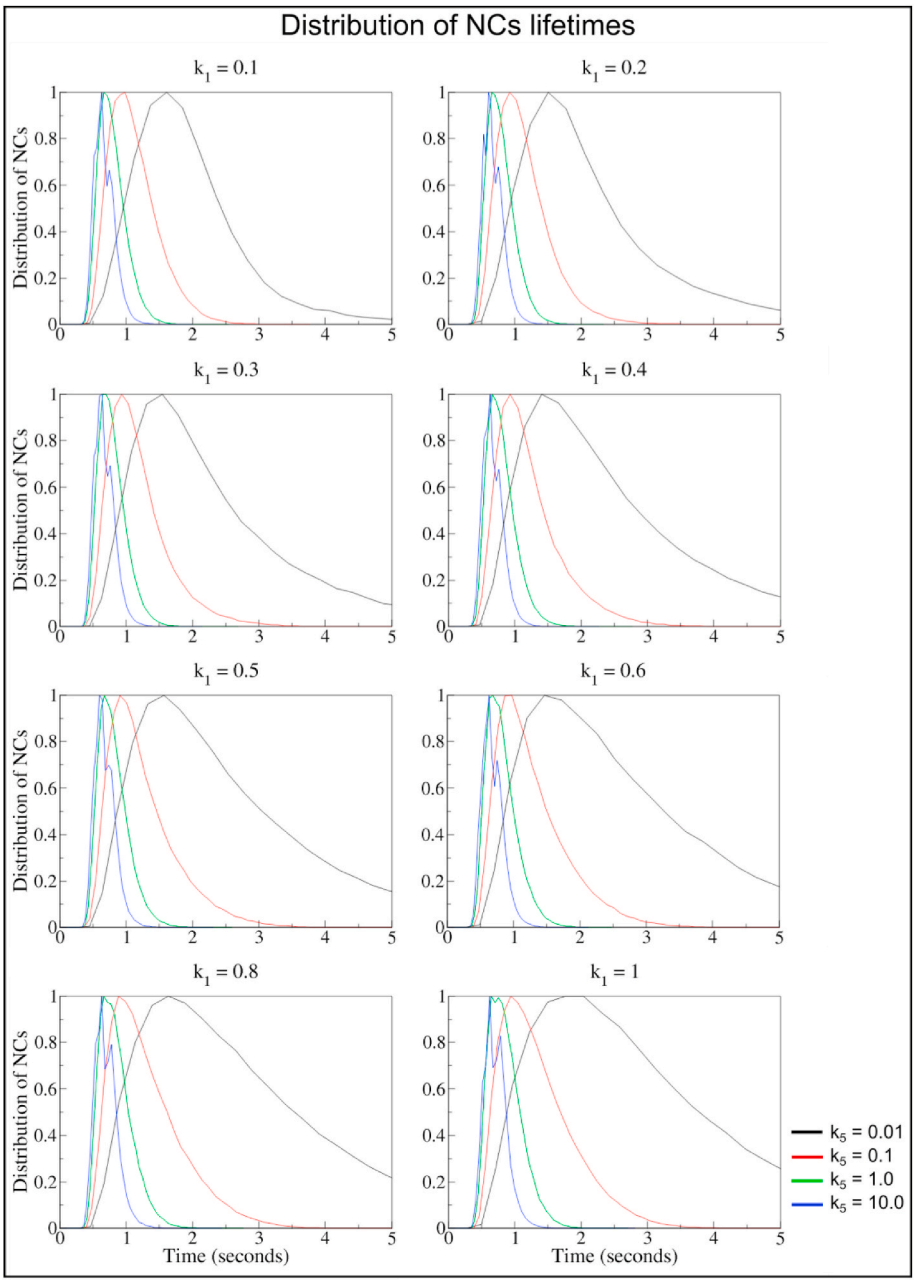

Fig. 7. Distribution of K-Ras NCs according to their lifetimes for variable k_5 values. Relative concentrations of active K-Ras NCs according to their lifetimes, from their generation until their disassembly. Each graph represents the distribution of the K-Ras NCs for a fixed value of k_1 within the range [0.1–1.0] s^{-1}. From each graph, every different distribution of K-Ras NCs (each color line) is related to a distinct value of k_5 within the range [0.01–10.0] s^{-1}. The relative concentrations of K-Ras NCs for a specific lifetime "i" are calculated as the ratio between the number of K-Ras NCs with a lifetime "i" and the maximum number of K-Ras NCs obtained among all available lifetimes (color version required for printing).

results fit with experimental findings that report the existence of a pool of active K-Ras dimers together with a great extension of active K-Ras NCs constituted by 3–10 protein kinase molecules, and with lifetimes close to 0.5 s [35,42,49,50,65–68].

Therefore, the proposed model evidence high robustness against shifts in the kinetic parameters (k_1 and k_5), and the oscillations in the growth/decrease of the NCs sizes may be responsible of it. Such oscillations are triggered by the high cooperativity of these nanostructures, and the dependence of their growth/decay reactions on their current sizes (oscillations do not arise if the reactions were defined through fixed kinetic constants; see Suppl. Fig. 9 for more detail).

Going into more detail, the simulations showed that the lifetime's distribution of the K-Ras NCs can be reduced, setting it close to the expected τ, as the rate of the K-Ras NC death reaction increases (Fig. 7). Such behavior is due to the relevance that k_5 provides to the K-Ras NC decay probability, increasing it until a scenario where a minimum local production of $_{pp}$ERK-1/2 is required for the nanostructure to self-regulate its own lifetime (i.e. leading to a high death probability from the time of producing at least one $_{pp}$ERK-1/2 molecule). However, k_1 has low relevance in lifetimes distributions of K-Ras NCs, since this rate directly regulates the formation of nanostructures but not their growth. What can be highlighted is a slight spread out of the distributions as k_1 increases (Fig. 8), mainly because an increase in the formation rate of K-Ras NCs triggers the generation of an important extension of these nanostructures with low sizes, which requires more time to grow and to produce enough local $_{pp}$ERK-1/2 responsible of self-regulating their own

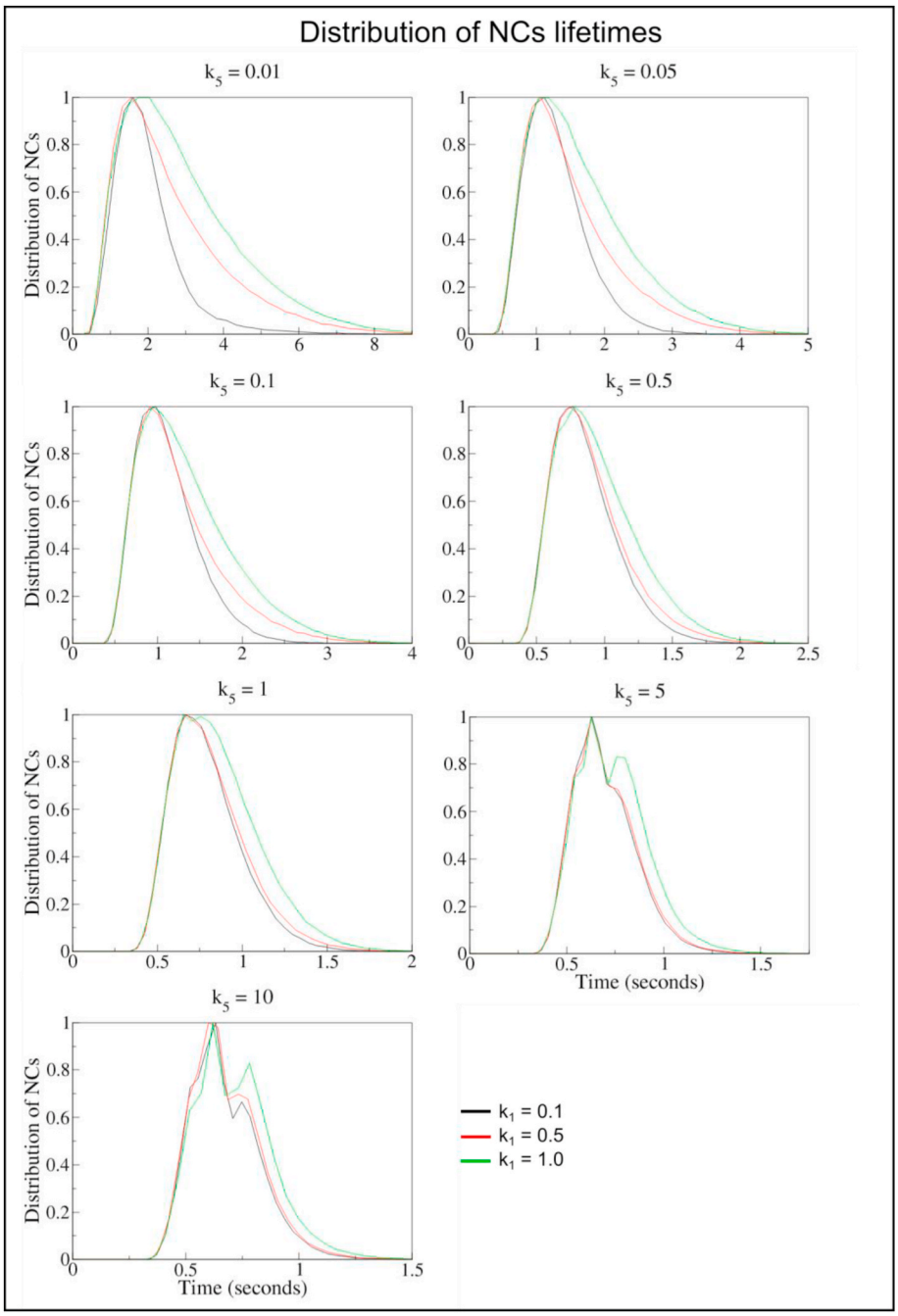

Fig. 8. Distribution of K-Ras NCs according to their lifetimes for variable k_1 values. Relative concentrations of active K-Ras NCs according to their lifetimes, from their generation until their disassembly. Each graph represents the distribution of the K-Ras NCs for a fixed value of k_5 within the range [0.01–10.0] s^{-1}. From each graph, every different distribution of K-Ras NCs (each color line) is related to a distinct value of k_1 within the range [0.1–1.0] s^{-1}. The relative concentrations of K-Ras NCs for a specific lifetime "i" are calculated as the ratio between the number of K-Ras NCs with a lifetime "i" and the maximum number of K-Ras NCs obtained among all available lifetimes (color version required for printing).

lifetimes.

On the other hand, increasing k_5, more K-Ras NCs with lower sizes, below the N_{sig}, and shorter lifetimes should coexist since less local $_{pp}$ERK-1/2 production is enough to self-regulate this last parameter (the local ppERK-1/2 expression is proportional to the NC size). However, the reported oscillations in the sizes distributions appear for the whole range of k_5 values, keeping the nanostructures within a controlled number of K-Ras kinases (Fig. 9). Instead, high rates of K-Ras NCs generation (k_1) lead to a high expression of such nanostructures with low sizes, capable of growing, from early moments of the simulation (Fig. 10). Consequently, a discrete expression of K-Ras monomers persists to be recruited by the existing K-Ras NCs that try to increase their sizes. At this point, whilst the pool of active K-Ras monomers decreases and the rate of nanostructures generation becomes slower, the generation of $_{pp}$ERK-1/2 and the chances of dissociation increase, even if much of the K-Ras NCs do not reach relevant sizes (far from the expected N_{sig}).

Therefore, the model provides evidence that both the size and lifetime of NCs can be tuned in a controlled manner by shifts in the kinetic parameters k_1 and k_5, but avoiding an uncontrolled spread on their distributions.

The EGF\K-Ras\ERK-1/2 MAPK pathway is up regulated in human

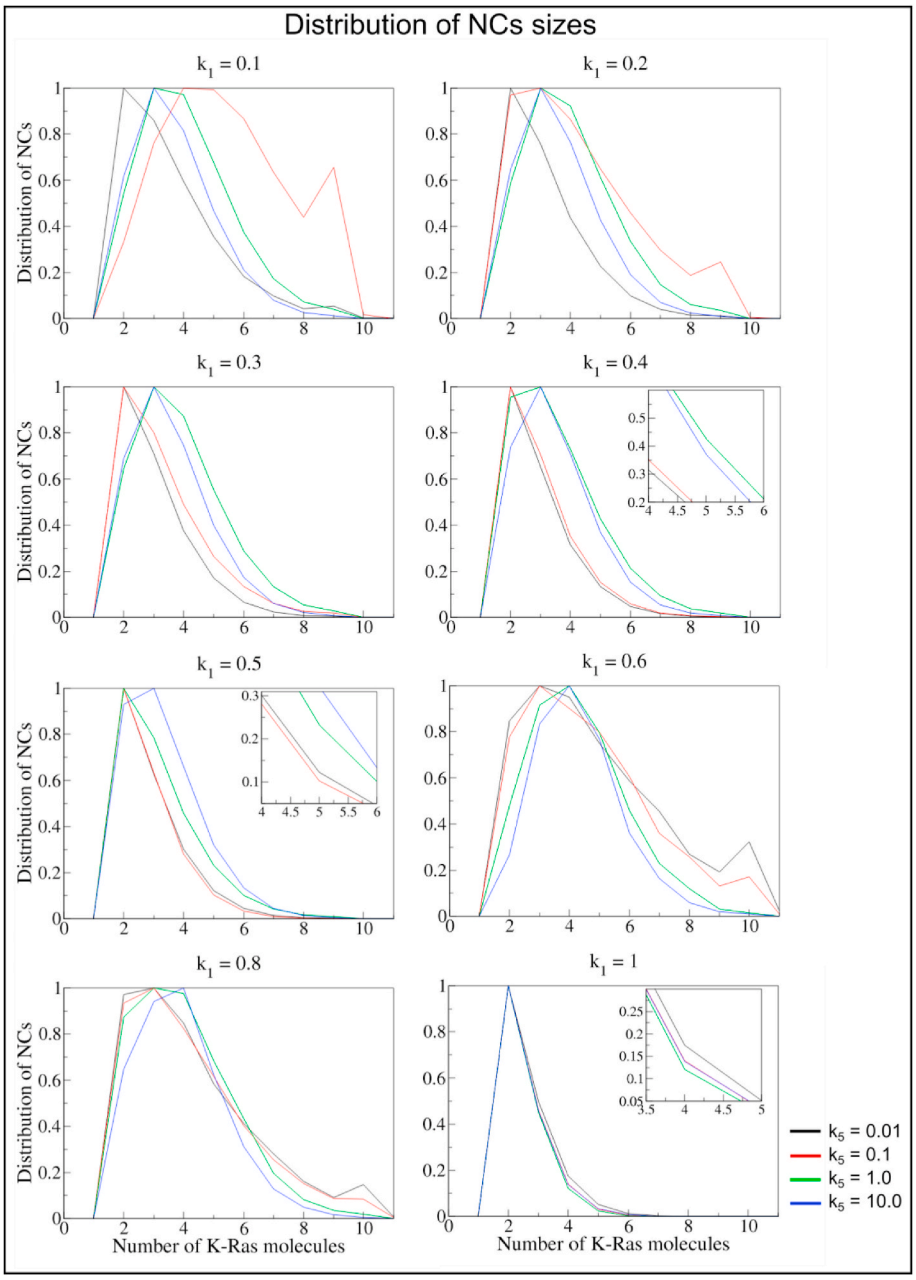

Fig. 9. Distribution of K-Ras NCs according to their sizes at disassembly time for variable k_5 values. Relative concentrations of active K-Ras NCs according to their sizes (number of clustered K-Ras kinases) at disassembly time. Each graph represents the distribution of the K-Ras NCs for a fixed value of k_1 within the range [0.1–1.0] s^{-1}. And from each graph, every different distribution of K-Ras NCs (each color line) is related to a distinct value of k_5 within the range [0.01–10.0] s^{-1}. The relative concentrations of K-Ras NCs for a specific size "i" are calculated as the ratio between the number of K-Ras NCs with size "i" and the maximum number of K-Ras NCs obtained among all available sizes (color version required for printing).

tumors, and blocking its signaling cascade in any of its steps is a potentially interesting approach in cancer therapy [6,69]. An increase in Ras concentration in nanoclusters promotes a hyperactivation of Ras signaling and tumorigenic growth [70]. Indeed, augmented K-Ras signal has been documented in breast cancer cells, which may be directly related to the level of K-Ras nanoclustering [71]. Considering that the local $_{pp}$ERK production of each K-Ras NC is proportional to its number of clustered K-Ras proteins [2], a link between the presence of tumor growth and the size of K-Ras nanoclusters may exist. Furthermore, since the growth/decay processes and the local production of a K-Ras NC may depend directly on its size, the regulation of such parameter opens the possibility to develop strategies to fight against cell diseases, such as tumor growth, modulating and limiting the expression of the $_{pp}$ERK-1/2 responsible of undesirable activation states of the cell response.

It is extensively reported that K-Ras is the most common oncogenic gene with the highest mutation rate among a huge variety of human cancers [72,73], being presented in approximately 25% of tumors, including very aggressive ones such as colorectal cancer, lung cancer, and pancreatic ductal adenocarcinoma. K-Ras is an attractive target for cancer therapy and thereby, huge efforts are focused on the development of cancer treatment strategies such as the design of specific inhibitors for free K-Ras mutants and its downstream signaling effectors, in order to prevent an undesirable K-Ras activation and signal [74–81]. Most of these strategies have been unsuccessful due to a lack of activity and target selectivity. For this reason, there is an urgent need for continuous investment and search in K-Ras-driven cancer strategies. At

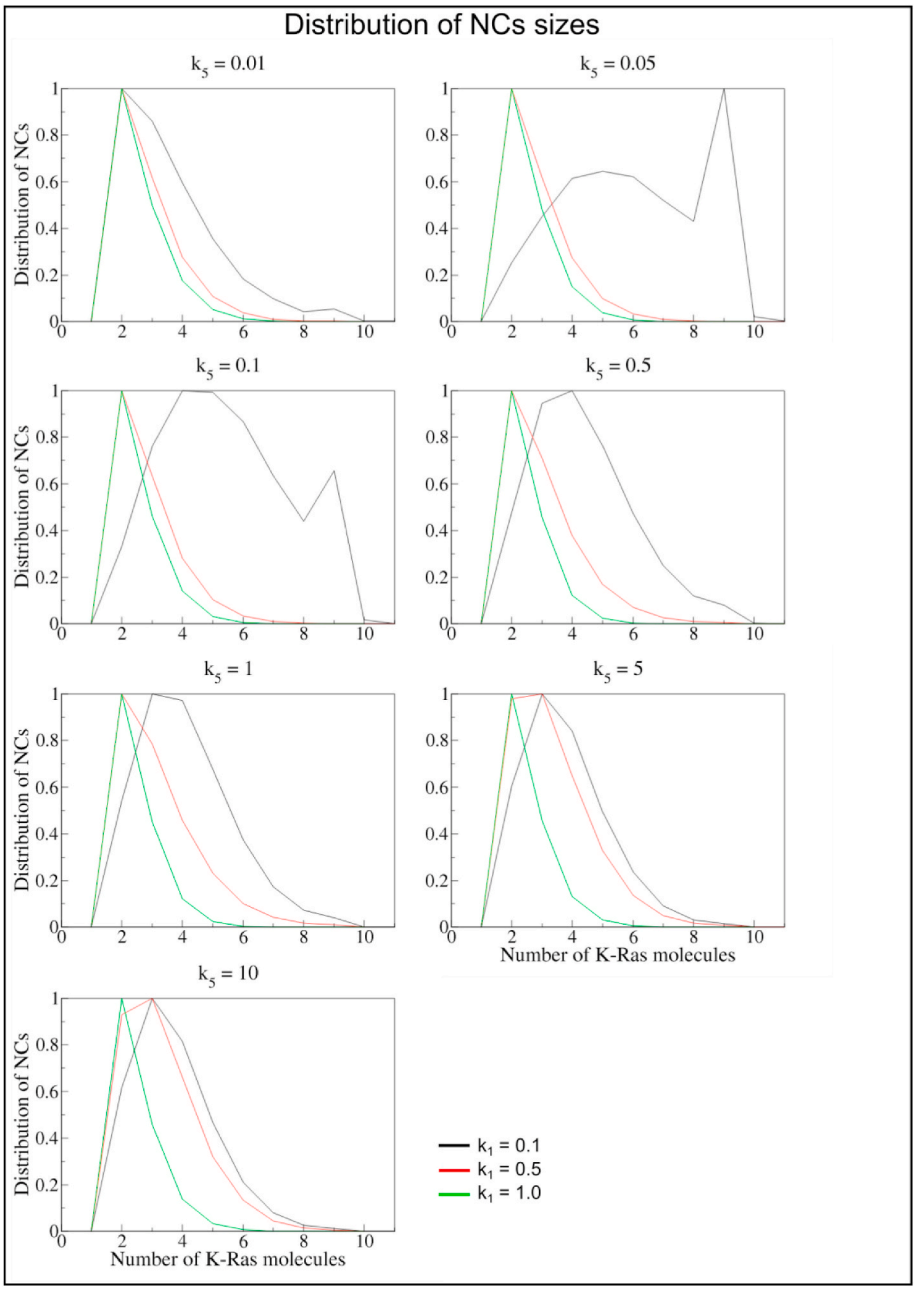

Fig. 10. Distribution of K-Ras NCs according to their sizes at disassembly time for variable k_1 values. Relative concentrations of active K-Ras NCs according to their sizes (number of clustered K-Ras kinases) at disassembly time. Each graph represents the distribution of the K-Ras NCs for a fixed value of k_5 within the range [0.01–10.0] s^{-1}. And from each graph, every different distribution of K-Ras NCs (each color line) is related to a distinct value of k_1 within the range [0.1–1.0] s^{-1}. The relative concentrations of K-Ras NCs for a specific size "i" are calculated as the ratio between the number of K-Ras NCs with size "i" and the maximum number of K-Ras NCs obtained among all available sizes (color version required for printing).

this point, the proposed model suggests that the signaling and the high fidelity of K-Ras NCs, as well as their growth/decay dynamics, largely depend on their sizes. The regulation of this parameter may allow modulating the signaling of the EGF\K-Ras\ERK-1/2 MAPK route in order to avoid cell damage and diseases.

4.1. Validation of results

The close match between the results generated from the proposed model's simulations and the experimental findings presented in the published literature is the primary evidence for validating the suggested model [4,6,11–13,42,49,50]. Indeed, the published results confirm that the distribution of the NCs' lifetimes is centered around 0.5 s and that the distribution of their sizes is ranged between 5 and 10 K-Ras molecules [4,6,11–13,42,49,50]. Surprisingly, the distributions of the lifetimes of the simulated NCs were centered between 0.5 and 1.0 s for $k_5 \geq 0.5\ s^{-1}$, regardless of the value of k_1 (considering the range defined in this study (Suppl. Table II). The distribution of the NCs sizes compressed in the experimental ranges is obtained with values of $k_5 \geq 0.1\ s^{-1}$ and $k_1 \leq 0.6\ s^{-1}$. Notice that the fitting of the obtained results from simulations with published studies is obtained for a wide range of kinetic values regarding k_1 and k_5, without fixing other kinetic parameters (k_2, k_3, and k_4 are defined as variables depending on the current NC size) and defining the proposed model of the growth/decay of NCs with the minimum number of basic reactions, avoiding complex signaling cascade structures and entanglement of reactions.

Furthermore, to evidence the suitability of the proposed model, simulations were run with fixed values of the kinetic parameters (k_2, k_3, k_4), rather than defining them as a function of the NC size (Suppl. Table IV). The obtained results are not as accurate as those provided by the proposed model when the internal kinetics are defined as a function of the current NC size. As a result, the lifetimes' distributions of the NCs spread out, moving away from the expected results in most combinations of these values. Even the sizes of the k-Ras NCs remain concentrated to low values for a wide range of the kinetic values (Suppl. Fig. 9). Therefore, the model with kinetic parameters defined with fixed values does not match with the realistic behavior of these types of NCs observed in experimental research, in addition to losing the robustness against shifts in the kinetic parameters.

4.2. Uncertainty analysis

Uncertainty analysis of obtained results has been performed based on the standard deviations from NCs distributions for some values of their sizes (2, 4, 6, 8, and 10 K-Ras) and for some values of their lifetimes (0.5, 0.75, 1.0, and 2.0 s), considering different values of k_1 and k_5 within their defined ranges.

Indeed, when discussing the sizes and lifetimes of K-Ras NCs, the values to be considered cover a wide range. Then, if the standard deviation of the distribution of NCs for each of the considered values of sizes and lifetimes is calculated considering the whole ranges of the kinetic parameters k_1 and k_5, important levels of dispersion of the results are obtained for both the sizes and lifetimes data sets (from 0.004 to 0.34 in the NCs distributions according to their sizes, and from 0.24 to 0.39 in the NCs distributions according to their lifetimes). The reason is that the distributions for each value of size and lifetime can vary depending on the value of the kinetic parameter. As a result, the higher the standard deviation, the more spread out the NCs distributions. When discussing the sizes and lifetimes of K-Ras NCs, there are a wide range of values to consider. For this reason, a more accurate analysis of the uncertainty in the results has been performed in detail considering the distributions of NCs for all different values of k_5 at each considered size value, as well as for all different values of k_1 at each considered value of lifetime. This option seems reasonable because the distribution of NCs in terms of size shows less dispersion for shifts in k_5 (Fig. 9). At the same time, the distribution of NCs concerning their lifetimes behave similarly when k_1 is varied (Fig. 8). In these cases, the standard deviation present low values in general trends, revealing that both the sizes and lifetimes of NCs are concentrated near the mean, presenting low dispersion in their distributions (Suppl. Tables V and VI, respectively). Thus, for the distribution of NCs according to their sizes, most of the standard deviations are below 0.02 but also appears some deviations ranged between (0.18–0.32). In the case of the distributions of NCs according to their lifetimes, most calculated deviations are below 0.12, except for three scenarios where the deviations are compressed within the range (0.10–0.13).

This analysis reinforces the idea that NC K-Ras have limited sizes and lifetimes in well-defined ranges, as reported in empirical evidence in the literature, as well as the results obtained from the simulations of the proposed model.

4.3. Model limitations and assumptions

The main limitation of the proposed model is that constitutes a simplified version of the three-step EGF\K-Ras\ERK-1/2 MAPK signaling route [14,15], and mainly accounts for the reactions involved in the growth and decay processes of K-Ras NCs, avoiding details of other processes such as the double phosphorylation that is driven when the different kinases of the signal transduction pathway are activated by their corresponding upstream protein. Therefore, the other reactions that are part of the signal transduction pathway can influence the considered reactions in the proposed model, even altering the speed and probability of occurrence of them. Of course, this assumption could be corrected by varying the speed of the reactions, and this effect was introduced in the proposed model when considering a spread range of values of the kinetic parameters k_1 and k_5.

Another assumption that presents the proposed signaling model is its isolation from other signaling pathways and motifs that coexist in the same cell environment. It is well known the crosstalk between the K-Ras signaling route and other pathways, such as the phosphatidylinositol 3-kinase (PI3K) pathway, the protein kinase B (AKT) pathway, the Ras homolog family member A (RhoA) pathway, and the mechanistic target of rapamycin (mTOR) [82,83]. This crosstalk describes the process that occurs inside a cell when specific signaling components are shared between different signaling pathways, or when a component from a signaling pathway is modified by the activity of one or some enzymes in another pathway. Indeed, crosstalk between two pathways results in different cell responses than that triggered by each pathway independently. For example, the K-Ras\ERK-1/2 and the PI3K-mTORC1 pathways crosstalk to both positive (cross-activation) and negative (cross-inhibition) regulation of each other [84]. Thus, the Ras/ERK pathway promotes mTOR activity and signaling through Raptor phosphorylation upon stimulation with EGF [85], but also negatively regulates the association of the Grb2-associated binder-1 (Gab1) with PI3K, which increases the PI3K activity [86]. However, inhibition of the PI3K \AKT\mTOR activity triggers Ras\MEK\ERK signaling in prostate cancer [87]. Even these pathways converge to act on the same substrate to trigger specific cell responses, such in the case of regulating the forkhead box O (FOXO) and c-Myc transcription factors [88,89].

Furthermore, there exist natural inhibitors of K-Ras signal that can block its activation and further clustering, affecting negatively the signal transduction through the MAPK route and influencing the cell fate. Some examples are the galectin-7 (Gal7) [90] and the protein arginine methyltransferase 5 (PRMT5) [91,92]. However, promoters of K-Ras activation also exist, which can accelerate the clustering and local production of these kinds of NCs, such as in the case of galectin-1 (Gal1) and −3 (Gal3) [93,94].

In addition, other molecules within the cell environment can interact with the signal transduction process of the EGF\K-Ras\ERK-1/2 MAPK pathway, altering its kinetic dynamics and the local $_{pp}$ERK production. One example is the scaffold proteins, which regulate several steps of the transduction process within the pathway, promoting its signal and local production when driving specific substrate into the pathway for its activation. Thus, MEK1 scaffolding protein (MP1) retains MEK and ERK at late endosomes, and it is required for sustained ERK activity. And kinase suppressor of Ras (KSR) MAPK scaffold translocates from the cytoplasm to the cell membrane in response to growth factors, driving the co-localization of RAF, MEK, and ERK needed for ERK activation [95,96].

All these interrelations from other signaling pathways and molecules can influence the growth and decay dynamics of K-Ras NCs. At this point, the aforementioned derived positive and negative effects may be assumed through variations in the kinetic parameters k_1 and k_5.

For example, the effect derived from the cross-inhibition of the K-Ras \ERK pathway through the interaction of the PI3K-mTORC1 pathway could be triggered by a decrease in the generation rate of K-Ras NCs, lowering the value of k_1. However, a limited scaffolding of Raf, MEK and ERK into the K-Ras NC would affect its local production and thereby, the probability of dye would decrease. And this effect would be reflected by means of lower k_5 values.

Another important point to consider in the model is the existence of a boundary condition regarding the expected size (N_{sig}), which is fixed to its maximum value of 10 K-Ras molecules in the present study, but it is related to experimental values ranging from 5 to 10 K-Ras molecules [35,50]. However, the causes that govern the existence of an optimal value of K-Ras NCs sizes remain unknown. Some evidences show the existence of an interaction between the K-Ras and some components of the cytoskeleton, such as flotillins, caveolins, actin, and tubulin, which

act as scaffolding proteins [3], inducing transient cluster formation, dissociation and localization [48]. Indeed, associations of membrane signaling domains (such as lipid rafts) with cytoskeleton proteins have been experimentally reported [3,97], where both cytoskeleton proteins and their membrane-associated targets undergo specific redistributions of their ensembles. Such structural redistributions influence, in turn, how signaling takes place [3]. In the specific case of a K-Ras NC, the orientation of its structural components is important for performing cell signaling. Thus, Raf monomers must be correctly oriented concerning Ras in order to shift to a dimer-favored state, which is required for activation [98,99]. That Raf orientation influences downstream signaling, promoting interactions between Raf and both the scaffolding proteins kinase suppressor of Ras (KSR) [100] and the IQ Motif Containing GTPase Activating Protein 1 (IQGAP1) [101,102]. In turn, depending on its orientation, IQGAP1 interacts with scaffolding proteins actin and tubulin [103]. In addition, perturbing the actin cytoskeleton affects Ras nanoclustering. Experiments showed that depleting cortical actin with latrunculin inhibits K-Ras clustering [42,104]. Moreover, cortical actin regulates the plasma membrane phosphatidylserine, and the disruption of actin by latrunculin increases the phosphatidylserine level in the plasma membrane that is available for interacting with K-Ras. As a result, a decrease of K-Ras lateral segregation is triggered and thereby, a reduction of its clustering arises [105,106].

At this point, it may be suggested that cytoskeleton can influence the regulation of a K-Ras NC ensemble and its size, but more studies in this line are required to clarify this paradigm. What is certain is that clustering takes place through binding events, which redistribute the ensemble, perturbing the structural conformation across the molecule. As a result, changes in one side of the cell can be reflected in another site, which is the basis of cooperativity [3].

5. Conclusion

The proposed model approach for the growth/decay dynamics of the K-Ras NCs within the EGF\K-Ras\ERK-1/2 MAPK signaling pathway considers the K-Ras NCs as cooperative structures that promote their own growth and local $_{pp}$ERK production and introduces novel and unusual manner of defining the inner kinetics of this signaling system, as variables that depend on the current NC size. This revolutionary kinetic approach to the signaling system allows us to avoid fixing values of the reaction rates, which may be difficult to determine, while revealing that this kind of systems are self-regulated.

Obtained results from simulations evidence the existence of an oscillatory pattern in the growth/decay dynamics of the K-Ras NCs that keep their sizes and lifetimes distributions between controlled values that fit largely with previously observed experimental results, for a wide range of kinetic parameters, revealing high levels of robustness.

Therefore, this new approach to defining NCs proposes their size as a key factor to regulate cell signaling, presenting new possibilities to develop strategies for use in chronic diseases and cancer.

Declaration of competing interest

The authors declare that they have no known competing financial interests or personal relationships that could have appeared to influence the work reported in this paper

Acknowledgments

This study was supported by research grants from the MICINN (SAF2016-75246R, RTI2018-097038-B-C22y, PID2021-124575OB-I00), the Generalitat de Catalunya (Grant 2017SGR1015), CIBERDEM ("Instituto de Salud Carlos III") and The European Commission (Horizon-EIC-2021-Pathfinderopen-01 101047099-4-DBR). A.Z. is a recipient of an ICREA "Academia" Award (Generalitat de Catalunya). We gratefully acknowledge institutional funding from the MINECO through the Centres of Excellence Severo Ochoa Award CEX2019-000913-S, and from the CERCA Programme of the Generalitat de Catalunya.

Appendix A. Supplementary data

Supplementary data to this article can be found online at https://doi.org/10.1016/j.compbiomed.2023.107455.

References

[1] U.S. Bhalla, R. Iyengar, Emergent properties of networks of biological signaling pathways, Science 283 (1999) 381–387.
[2] M.A. Serrano, M. Jurado, R. Reigada, Negative-feedback self-regulation contributes to robust and high-delity transmembrane signal transduction, J. R. Soc. Interface 10 (88) (2013), 20130581.
[3] R. Nussinov, H. Jang, C.-J. Tsai, Oligomerization and nanocluster organization render specificity, Biol. Rev. Camb. Phil. Soc. 90 (2) (2015) 587–598.
[4] Q.N. Van, et al., RAS nanoclusters: dynamic signaling platforms amenable to therapeutic intervention, Biomolecules 11 (2021) 377.
[5] R. Nussinov, B. Ma, C.J. Tsai, A broad view of scaffolding suggests that scaffolding proteins can actively control regulation and signaling of multienzyme complexes through allostery, Biochim. Biophys. Acta 1834 (2013) 820–829.
[6] E.S. Ozdemir, A.M. Koester, X. Nan, Ras multimers on the membrane: many ways for a heart-to-heart conversation, Genes (Basel) 13 (2) (2022) 219.
[7] A. Kusumi, et al., Hierarchical mesoscale domain organization of the plasma membrane, Trends Biochem. Sci. 36 (2011) 604–615.
[8] E. Sezgin, I. Levental, S. Mayor, C. Eggeling, The mystery of membrane organization: composition, regulation and roles of lipid rafts, Nat. Rev. Mol. Cell Biol. 18 (2017) 361–374.
[9] Y.I. Henis, J.F. Hancock, I.A. Prior, Ras acylation, compartmentalization and signalling nanoclusters, Mol. Membr. Biol. 26 (1) (2009), 8092.
[10] B.N. Kholodenko, J.F. Hancock, W. Kolch, Signalling ballet in space and time, Nat. Rev. Mol. Cell Biol. 11 (2010), 414426.
[11] A.S. Harding, J.F. Hancock, Using plasma membrane nanoclusters to build better signaling circuits, Trends Cell Biol. 18 (2008), 364371.
[12] E. Roob III, N. Trendel, P. Rein ten Wolde, A. Mugler, Cooperative clustering digitizes biochemical signaling and enhances its fidelity, Biophys. J. 110 (2016), 16611669.
[13] Y. Zhou, J.F. Hancock, Ras nanoclusters: versatile lipid-based signaling platforms, Biochim. Biophys. Acta 1853 (2015) 841–849.
[14] C.Y. Huang, J.E. Ferrell, Ultrasensitivity in the mitogen-activated protein kinase cascade, Proc. Natl. Acad. Sci. USA 93 (1996).
[15] O.E. Sturm, et al., The mammalian MAPK/ERK pathway exhibits properties of a negative feedback amplifier, Sci. Signal. 3 (2010) ra90.
[16] K.-Y. Lee, et al., Oncogenic KRAS G12D mutation promotes dimerization through a second, phosphatidylserine–dependent interface: a model for KRAS oligomerization, Chem. Sci. 12 (2021), 12827.
[17] T.S. Lewis, P.S. Shapiro, N.G. Ahn, Signal transduction through MAP kinase cascades, Adv. Cancer Res. 74 (1998), 49139.
[18] B. Errede, et al., Dynamics and organization of MAP kinase signal pathways, Mol. Reprod. Dev. 42 (1995), 477485.
[19] M.J. Robinson, M.H. Cobb, Mitogen-activated protein kinase pathways, Curr. Opin. Cell Biol. 9 (1997), 180186.
[20] H.J. Schaeffer, M.J. Weber, Mitogen-activated protein kinases: specific messages from ubiquitous messengers, Mol. Cell Biol. 19 (1999), 24352444.
[21] L. Chang, M. Karin, Mammalian MAP kinase signaling cascades, Nature 410 (2001) 37–40.
[22] G. Pearson, et al., Mitogen-activated protein (MAP) kinase pathways: regulation and physiological functions, Endocr. Rev. 22 (2) (2001), 153183.
[23] M. Raman, W. Chen, M.H. Cobb, Differential regulation and properties of MAPKs, Oncogene 26 (2007) 3100–3112.
[24] M. Cargnello, P.P. Roux, Activation and function of the MAPKs and their substrates, the MAPK-Activated Protein Kinases, Microbiol. Mol. Biol. Rev. 5083 (2011).
[25] K. Inder, et al., Activation of the MAPK module from different spatial locations generates distinct system outputs, Mol. Biol. Cell 19 (2008), 47764784.
[26] B. Schoeberl, C. Eichler-Jonsson, E.D. Gilles, G. Muller, Computational modeling of the dynamics of the MAP kinase cascade activated by surface and internalized EGF receptors, Nat. Biotechnol. 20 (2002) 370–375.
[27] P.P. Roux, J. Blenis, ERK and p38 MAPK-activated protein kinases: a family of protein kinases with diverse biological functions, Microbiol. Mol. Biol. Rev. (2004), 320344.
[28] M.K. Dougherty, et al., Regulation of Raf-1 by direct feedback phosphorylation, Mol. Cell 17 (2005) 215–224.
[29] K.L. Yee, V.M. Weaver, D.A. Hammer, Integrin-mediated signalling through the MAP-kinase pathway, IET Syst. Biol. 2 (1) (2008) 8–15.
[30] L. Buday, J. Downward, Epidermal growth factor regulates p21 ras through the formation of a complex receptor, Grb2 adaptor protein and Sos nucleotide exchange factor, Cell 48 (1993), 611620.
[31] R.J. Orton, et al., Computational modelling of the receptor-tyrosine-kinase-activated MAPK pathway, Biochem. J. 392 (2005), 249261.
[32] S.L. Campbell, et al., Increasing complexity of Ras signaling, Oncogene 17 (1998), 13951413.

[33] K. Wood, C. Sarnecki, T.M. Roberts, J. Blenis, c-Ras mediates nerve growth factor receptor modulation of three signal-transducing protein kinases: MAP kinase, Raf-1 and RSK, Cell 68 (1992), 10411050.
[34] M. Geyer, A. Wittinghofer, GEFs, GAPs, GDIs and effectors: taking a closer (3D) look at the regulation of Ras-related GTP-binding proteins, Curr. Opin. Struct. Biol. 7 (1997) 786–792.
[35] S.J. Plowman, et al., Electrostatic interactions positively regulate K-Ras nanocluster formation and function, Mol. Cell Biol. (2008) 4377–4385.
[36] T. Gurry, Kahramanogullari, R.G. Endres, Biophysical mechanism for Ras-nanocluster formation and signaling in plasma membrane, PLoS One 4 (7) (2009), e6148.
[37] D. Abankwa, A.G. Alemayehu, J. Hancock, Ras nanoclusters: molecular structure and assembly, Semin. Cell Dev. Biol. 18 (2007), 599607.
[38] C. Hagemann, U.R. Rapp, Isotype-specific functions of Raf kinases, Exp. Cell Res. 253 (1) (1999) 34–46.
[39] D.K. Morrison, R.E. Cutler, The complexity of Raf-1 regulation, Curr. Opin. Cell Biol. 9 (2) (1997) 174–179.
[40] F.A. Brightman, D.A. Fell, Differential feedback regulation of the MAPK cascade underlies the quantitative differences in EGF and NGF signaling in PC12 cells, FEBS (Fed. Eur. Biochem. Soc.) Lett. 482 (2000) 169–174.
[41] S.-Y. Shin, O. Rath, S.-M. Choo, F. Fee, B. McFerran, W. Kolch, K.-H. Cho, *Positive and negative feedback regulations coordinate the dynamic behavior of the Ras-Raf-MEK-ERK signal transduction pathway*, J. Cell Sci. 122 (2009) 425–435.
[42] S.J. Plowman, C. Muncke, R.G. Parton, J.F. Hancock, H-ras, K-ras, and inner plasma membrane raft proteins operate in nanoclusters with differential dependence on the actin cytoskeleton, Proc. Natl. Acad. Sci. U.S.A. 102 (2005) 15500–15505.
[43] F. Calvo, L. Agudo-Ibez, P. Crespo, The Ras-ERK pathway: understanding site-specic signaling provides hope of new anti-tumor therapies, Bioessays 32 (2010) 412–421.
[44] H.E. Sanchez-Ibarra, et al., KRAS, NRAS, and BRAF mutation prevalence, clinicopathological association, and their application in a predictive model in Mexican patients with metastatic colorectal cancer: a retrospective cohort study, PLoS One 15 (7) (2020), e0235490.
[45] I.A. Prior, F.E. Hood, J.L. Hartley, The frequency of Ras mutations in cancer, Cancer Res. 80 (14) (2020) 2696–2974.
[46] P. Castel, K.A. Rauen, F. McCormick, The duality of human oncoproteins: drivers of cancer and congenital disorders, Nat. Rev. Cancer 20 (7) (2020) 383–397.
[47] D. Abankwa, A.A. Gorfe, Mechanisms of Ras membrane organization and signaling: ras rocks again, Biomolecules 10 (2020), 1522.
[48] R. Nussinov, B. Ma, C.J. Tsai, A broad view of scaffolding suggests that scaffolding proteins can actively control regulation and signaling of multienzyme complexes through allostery, Biochim. Biophys. Acta 1834 (2013) 820–829.
[49] T. Tian, S.J. Plowman, R.G. Parton, Y. Kloog, J.F. Hancock, Mathematical modeling of K-Ras nanocluster formation on the plasma membrane, Biophys. J. 99 (2010) 534–543.
[50] T. Tian, et al., Plasma membrane nanoswitches generate high-fidelity Ras signal transduction, Nat. Cell Biol. 9 (8) (2007) 905–914.
[51] A. Sayyed-Ahmad, et al., Computational equilibrium thermodynamic and kinetic analysis of K-ras dimerization through an effector binding surface suggests limited functional role, J. Phys. Chem. B 120 (33) (2016) 8547–8556.
[52] A. Fujioka, et al., Dynamics of the Ras/ERK MAPK cascade as monitored by fluorescent probes, J. Biol. Chem. 281 (2006) 8917–8926.
[53] Y.-C. Li, et al., Analysis of RAS protein interactions in living cells reveals a mechanism for pan-RAS depletion by membrane-targeted RAS binders, Proc. Natl. Acad. Sci. USA 117 (22) (2020) 12121–12130.
[54] S. Muratcioglu, et al., GTP-dependent K-ras dimerization, Structure 23 (2015) 1325–1335.
[55] F. Ginot, I. Theurkauff, F. Detcheverry, C. Ybert, C. Cottin-Bizonne, Aggregation-fragmentation and individual dynamics of active clusters, Nat. Commun. 19 (2018) 696.
[56] Q. Vagne, M.S. Turner, P. Sens, Sensing size through clustering in nonequilibrium membranes and the control of membrane-bound enzymatic reactions, PLoS One 10 (12) (2015), e0143470.
[57] J. Wang, et al., Mapping allosteric communications within individual proteins, Nat. Commun. 11 (2020), 3862.
[58] S. Li, X. Zhang, W. Wang, Cluster Formation of anchored proteins induced by membrane-mediated interaction, Biophys. J. 98 (11) (2010) 2554–2563.
[59] J.C. Ezerski, M.S. Cheung, CATS: a tool for clustering the ensemble of intrinsically disordered peptides on a flat energy landscape, J. Phys. Chem. B 122 (49) (2018) 11807–11816.
[60] J.-C. Walter, et al., Looping and clustering model for the organization of protein-DNA complexes on the bacterial genome, New J. Phys. 20 (2018), 035002.
[61] D. Soraruf, et al., Protein cluster formation in aqueous solution in the presence of multivalent metal ions – a light scattering study, Soft Matter 10 (2014) 894–902.
[62] D.T. Gillespie, General method for numerically simulating stochastic time evolution of coupled chemical-reactions, J. Comput. Phys. 22 (1976), 403434.
[63] D.T. Gillespie, Exact stochastic simulation of coupled chemical reactions, J. Phys. Chem. 81 (25) (1977), 23402361.
[64] D.T. Gillespie, Stochastic simulation of chemical kinetics, Annu. Rev. Phys. Chem. 58 (2007), 3555.
[65] Y. Zhou, et al., Ras and the plasma membrane: a complicated relationship, Cold Spring Harb. Perspect. Med. 8 (2018), a031831.
[66] S. Sarkar-Banerjee, et al., Spatiotemporal analysis of K-Ras plasma membrane interactions reveals multiple high order homo-oligomeric complexes, J. Am. Chem. Soc. 139 (38) (2017) 13466–13475.
[67] A. Herrero, P. Crespo, Ras dimers: the novice couple at the Ras-ERK pathway ball, Genes 12 (2021), 1556.
[68] X. Nan, et al., Ras-GTP dimers activate the mitogen-activated protein kinase (MAPK) pathway, Proc. Natl. Acad. Sci. USA 112 (2015) 7996–8001.
[69] M. Kohono, J. Pouyssegur, Targeting the ERK signaling pathway in cancer therapy, Ann. Med. 38 (2006) 200–211.
[70] M. Solman, et al., Specific cancer-associated mutations in the switch III region of Ras increase tumorigenicity by nanocluster augmentation, Elife 4 (2015), e08905.
[71] R. Shalom-Feuerstein, et al., K-ras nanoclustering is subverted by overexpression of the scaffold protein galectin-3, Cancer Res. 68 (16) (2008) 6608–6616.
[72] I.A. Prior, P.D. Lewis, C. Mattos, A comprehensive survey of Ras mutations in cancer, Cancer Res. 72 (2012) 2457–2467.
[73] A.D. Cox, et al., Drugging the undruggable RAS: mission possible? Nat. Rev. Drug Discov. 13 (2014) 828–851.
[74] W. Liu, et al., Kras mutations increase telomerase activity and targeting telomerase is a promising therapeutic strategy for Kras-mutant NSCLC, Oncotarget 8 (2017) 179–190.
[75] R. Srikar, et al., Targeted nanoconjugate co-delivering siRNA and tyrosine kinase inhibitor to KRAS mutant NSCLC dissociates GAB1-SHP2 post oncogene knockdown, Sci. Rep. 6 (2016), 30245.
[76] M. Puyol, et al., A synthetic lethal interaction between K-Ras oncogenes and Cdk4 unveils a therapeutic strategy for non-small cell lung carcinoma, Cancer Cell 18 (2010) 63–73.
[77] K. Sakamoto, T. Masutani, T. Hirokawa, Generation of KS-58 as the first K-Ras (G12D)-inhibitory peptide presenting anti-cancer activity in vivo, Sci. Rep. 10 (2020), 21671.
[78] K.M. McAndrews, et al., Exosome-mediated delivery of CRISPR/Cas9 for targeting of oncogenic Kras in pancreatic cancer, Life Sci. Alliance 4 (2021), e202000875.
[79] K.W. Teng, et al., Selective and noncovalent targeting of RAS mutants for inhibition and degradation, Nat. Commun. 12 (2021), 2656.
[80] S.J. Ross, et al., Targeting KRAS-dependent tumors with AZD4785, a high-affinity therapeutic antisense oligonucleotide inhibitor of KRAS, Sci. Transl. Med. 9 (2017), eaal5253.
[81] M. Sanclemente, et al., c-RAF ablation induces regression of advanced Kras/Trp53 mutant lung adenocarcinomas by a mechanism independent of MAPK signaling, Cancer Cell 33 (2018) 217–228, e4.
[82] E. Rozengurt, G. Eibl, Crosstalk between KRAS, SRC and YAP signaling in pancreatic cancer: interactions leading to aggressive disease and drug resistance, Cancers 13 (20) (2021), 5126.
[83] T.W. Chew, et al., Crosstalk of Ras and Rho: activation of RhoA abates Kras-induced liver tumorigenesis in transgenic zebrafish models, Oncogene 33 (2014) 2717–2727.
[84] M.C. Mendoza, E.E. Er, J. Blenis, The Ras-ERK and PI3K-mTOR pathways: cross-talk and compensation, Trends Biochem. Sci. 36 (6) (2011) 320–328.
[85] A. Carriere, et al., ERTK 1/2 phosphorylate raptor to promote Ras-dependent activation of mTOR complex 1 (mTORC1), Signal Transduct. 286 (1) (2011) 567–577.
[86] C.F. Yu, Z.X. Liu, Ll Cantley, ERK negatively regulates the epidermal growth factor-mediated interaction of Gab1 and the phosphatidylinositol 3-kinase, J. Biol. Chem. 277 (22) (2002) 19382–19388.
[87] D.E. Butler, et al., Inhibition of the PI3K/AKT/mTOR pathway activate autophagy and compensatory Ras/Raf/MEK/ERK signalling in prostate cancer, Oncotarget 8 (2017) 56698–56713.
[88] J.Y. Yang, et al., ERK promotes tumorigenesis by inhibiting FOXO3a via MDM2-mediated degradation, Nat. Cell Biol. 10 (2) (2008) 138–148.
[89] B.D. Manning, L.C. Cantley, AKT/PKB signaling: navigating downstream, Cell 129 (7) (2007) 1261–1274.
[90] B. Barkan, A.D. Cox, Y. Kloog, Ras inhibition boosts galectin-7 at the expense of galectin-1 to sensitize cells to apoptosis, Oncotarget 4 (2013) 256–268.
[91] P. Andreu-Pérez, et al., Protein arginine methyltransferase 5 regulates ERK1/2 signal transduction amplitude and cell fate through CRAF, Sci. Signal. 4 (190) (2011) ra58.
[92] M. Jurado, O. Castaño, A. Zorzano, Stochastic modulation evidences a transitory EGF-Ras-ERK MAPK activity induced by PRMT5, Comput. Biol. Med. 133 (2021), 104339.
[93] L.Y. Chung, et al., Galectin-1 promotes lung cancer progression and chemoresistance by upregulating p38 MAPK, ERK, and cyclooxygenase-2, Clin. Cancer Res. 18 (2012) 4037–4047.
[94] G. Elad-Sfadia, et al., Galectin-3 augments K-Ras activation and triggers a Ras signal that attenuates ERK but not phosphoinositide 3-kinase activity, J. Biol. Chem. 279 (2004) 34922–34930.
[95] M.M. McKay, D.K. Morrison, Integrating signals from RTKs to ERK/MAPK, Oncogene 26 (22) (2007) 3113–3121.
[96] S. Nada, et al., The novel lipid raft adaptor p18 controls endosome dynamics by anchoring the MEK-ERK pathway to late endosomes, EMBO J. 28 (5) (2009) 477–489.
[97] R. Nussinov, The spatial structure of cell signaling systems, Phys. Biol. 10 (2013), 045004.
[98] H. Lavoie, M. Therrien, Cancer: a drug-resistant duo, Nature 480 (2011) 329–330.
[99] P.I. Poulikakos, et al., RAF inhibitor resistance is mediated by dimerization of aberrantly spliced BRAF(V600E), Nature 480 (2011) 387–390.
[100] C.M. Udell, et al., Mechanistic principles of RAF kinase signaling, Cell. Mol. Life Sci. 68 (2011) 553–565.
[101] J.-G. Ren, Z. Li, D.B. Sacks, IQGAP1 modulates activation of B-Raf, Proc. Natl. Acad. Sci. USA 104 (25) (2006) 10465–10469.

[102] C.D. White, H.H. Erdemir, D.B. Sacks, IQGAP1 and its binding proteins control diverse biological functions, Cell. Signal. 24 (4) (2012) 826–834.
[103] S. Malarkannan, et al., IQGAP1: a regulator of intracellular spacetime relativity, J. Immunol. 188 (2012) 2057–2063.
[104] I.A. Prior, C. Muncke, R.G. Parton, J.F. Hancock, Direct visualization of Ras proteins in spatially distinct cell surface microdomains, J. Cell Biol. 160 (2003) 165–170.
[105] Y. Zhou, H. Liang, T. Rodkey, N. Ariotti, R.G. Parton, J.F. Hancock, Signal integration by lipid-mediated spatial cross talk between ras nanoclusters, Mol. Cell Biol. 34 (2014) 862–876.
[106] J.G. Kay, M. Koivusalo, X. Ma, T. Wohland, S. Grinstein, Phosphatidylserine dynamics in cellular membranes, Mol. Biol. Cell 23 (2012) 2198–2212.